Modeling Deformable Linear Objects for Autonomous Robotic Outfitting of Lunar Surface Systems

Amy M. Quartaro[1], John R. Cooper, Ph.D.[2], Joshua N. Moser, Ph.D.[3], and Erik. E. Komendera, Ph.D.[4]

[1]FASER Lab Graduate Research Assistant, Virginia Tech Mechanical Engineering Dept, Blacksburg, VA, 24060, United States, Contact: aquartaro@vt.edu
[2]Autonomous Integrated Systems Research Branch, NASA Langley Research Center, Hampton, VA, 23681, United States
[3]Autonomous Integrated Systems Research Branch, NASA Langley Research Center, Hampton, VA, 23681, United States
[4]Assistant Professor and FASER Lab Director, Virginia Tech Mechanical Engineering Dept, Blacksburg, VA, 24060, United States

ABSTRACT

The construction of in-space facilities is a significant capability for the establishment of a long-term human presence in space. Autonomous robotic technologies are a critical tool to enabling the construction and maintenance of such permanent facilities. This paper evaluates the outfitting portion of the construction process, focusing on modeling required for robotic manipulation of cable-like objects, referred to as Deformable Linear Objects (DLOs). DLOs contain a high degree of variability, which makes accurate real-time autonomous operations a difficult task. Different modeling methods for DLOs such as discrete mass-spring systems and Cosserat elastic rod models range in problem complexity and accuracy, a trade-off that must be understood to fully realize autonomous cable routing technologies. This paper validates different DLO models through simulation and a hardware experiment, highlighting the size of the state space and accuracy of different approaches. The development of DLO manipulation models for outfitting enables an autonomous architecture for the construction of lunar surface systems.

INTRODUCTION

A persistent human presence on the lunar surface is one of the next major milestones in space exploration. This paper investigates the modeling of cables for outfitting permanent facilities with robotic agents, a technology critical to construction and maintenance of lunar facilities but also not a well matured technology terrestrially.

Robust extraplanetary construction and manufacturing capabilities, including structures and materials modeling and robotic systems, have been identified as key areas for enabling lunar infrastructure (NASA 2022a). Previous robotic construction technology development has primarily focused on structural assembly, with significantly less focus on robotically performed outfitting tasks to instantiate subsystems providing power, data, life support, etc. These tasks involve manipulation of highly flexible elements, which are difficult to model, such as cable harnesses, ropes, and hoses.

Such flexible elements are a constant presence for space systems, such as the International Space Station (ISS) shown in Figure 1a. This paper presents structural models of deformable linear objects (DLOs). DLOs are a subclass of deformable objects that encompasses common outfitting elements such as cables and ropes. Models are validated through a hardware experiment, and integration in a robotic autonomy architecture for space environments is discussed. Robotic manipulation of DLOs, especially cable harnesses, is an active area of research as cable harnesses are essential for providing power and data to space assets. DLO models that can be used for robot manipulator trajectory generation are necessary for autonomous operation of lunar infrastructure. An example of robotic cable manipulation is shown in Figure 1b.

This paper evaluates two of the most common methods for modeling DLOs, position based multibody models and the more continuous Cosserat rod formulations, and compares them to a 2D hardware experiment. There is an evaluation of the state size of each model, exploration into the trade-off between different modeling approaches, and comparisons of accuracy and computational complexity of the formulation types mentioned above. Understanding the tradeoffs between different cable modeling techniques paves the way for developing robotic control and planning architectures necessary for real-time manipulation of DLOs. Real-time control is required for robotic systems to be able to actively manipulate a cable in a harsh environment where model and sensor errors compound, and environmental conditions can cause significant disturbances. Cable routing must be performed in areas with high density of objects/obstacles: through truss structures, near solar panels or mirror arrays, next to bundles of electrical equipment. Understanding the best way to plan and manipulate a cable without disrupting the environment or damaging the cable is imperative to robotic outfitting operations on the lunar surface.

The remainder of this paper further details applications of multibody and Cosserat rod formulations and compares the static solution to the results of a hardware experiment. The mathematical formulation for each model is described in detail and implemented in simulation. The simulations

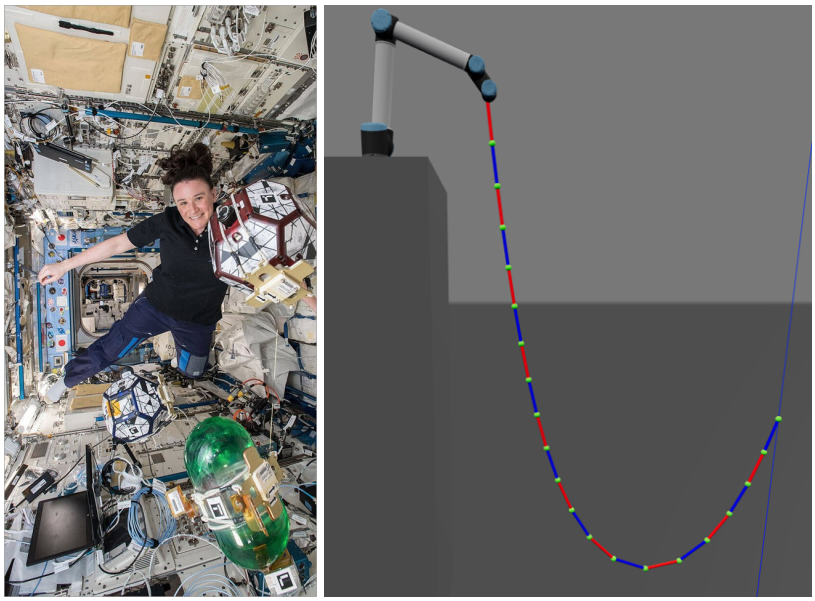

(a) **(b)**

Fig. 1. (a) DLOs on the ISS (Credit: NASA), (b) Robotic cable routing simulation

are then compared to evaluate the trade-off between the number of states and deviation from the hardware results for each model. Finally, steps required to incorporate the appropriate DLO model into an in-space outfitting scenario are discussed.

In-space construction

In-space assembly and construction has historically been a significant area of interest (Belvin et al. 2016). For a persistent lunar presence, such assembly and construction activities must leverage the use of robotic elements to reduce crew risk and maintain systems when crew is not present. There have been a variety of studies evaluating existing technologies for robotic lunar infrastructure (Waltz et al. 2022) (Govindaraj et al. 2019) (Moses and Mueller 2021), but the focus has primarily been on evaluating the overall architecture and feasibility of an integrated infrastructure. Whether erected from In-Situ Resource Utilization (ISRU) technologies (ICON Technology 2022), deployed components (NASA 2020) or delivered strut components (Song et al. 2023), concepts for robotic construction do not address the need for outfitting and maintenance once the structure is complete.

Autonomous robotic systems aiding in assembly and manufacturing provide a promising foundation for the level of autonomy necessary for a robotic agent to complete cable routing tasks. In a space environment, communication latencies and poor visual quality could impact an operator's ability to successfully maneuver a DLO without some degree of autonomy. Planning and state estimation for in-space construction and assembly systems have been evaluated for robotic teams (Everson et al. 2020), satellite servicing (NASA 2022b), and telescope assembly (Karumanchi et al. 2018). These endeavors for in-space robotics demonstrate the viability of leveraging autonomous techniques for in-space applications, paving the way for applying DLO manipulation techniques to in-space outfitting and maintenance applications.

DLO Modeling and Manipulation

Modeling and manipulating DLOs is a challenging robotics problem, complex in modeling and execution but extremely relevant to automation. The complexity of modeling DLOs varies based upon the application and desired accuracy, and has evolved into a significant field of research within the domain of deformable objects (Lv et al. 2020) (Sanchez et al. 2018). There are many proposed methods for modeling DLOs, and the trade-off between model accuracy and computational speed informs which type should be used. An understanding of this trade-off is imperative for real-time control of autonomous systems. High computational requirements reduce the speed of the model, making real-time control difficult, while accuracy is critical to preventing collisions.

Treating a DLO like a serially chained multibody model is one of the simplest ways to model a given cable. By defining the cable as rigid segments connected by linear and torsional springs and dampers, the total energy and forces in a cable can be determined using formulations as in multibody dynamics. This model is also referred to as the mass-spring approach. Such a method has been used to assist in multiple automation applications, including welding cable shape optimization (Suzuki et al. 2022), managing cables powering automation robotics themselves (Iwamura et al. 2022), and dual-arm manipulation and planning (Yu et al. 2023). Modeling a DLO with the multibody approach reduces the size of the state space, but the reliance on discretization reduces the accuracy of the model for complex systems.

In comparison to reducing a DLO into simpler components, Cosserat rod theory is a generalization of the inextensible Kirchoff rod and provides the basis for a high fidelity continuous model (Kugelstadt and Schömer 2016). Cosserat rods are popular for modeling DLOs and continuum

robots due the higher fidelity, but require a large number of states to track the DLO in an environment. There has been significant research in recent years into applying Cosserat theory for DLO manipulation; planning for ropes and wires (Liu et al. 2023) (Lv et al. 2022), tying knots (Saha and Isto 2007), and applications to automotive wiring harness installation (Hermansson et al. 2013). Tummers et al. (2023) and Gazzola et al. (2018) investigate different approaches with modeling continuum robots with a Cosserat formulation.

A Lagrangian energy formulation is often used to determine the physical shape of the cable. Since a cable at rest will have minimal potential energy, optimization techniques can be used to model a static cable (Moll and Kavraki 2006). The multibody formulation in this paper directly applies this concept, similar to other works (Suzuki et al. 2022) (Yu et al. 2023). Implementations of a Lagrangian energy solution can also be applied to a continuous Cosserat rod (Tummers et al. 2023) (Shah et al. 2018).

Additionally, in recent years there have been efforts into utilizing neural network approaches to DLO estimation (Jin et al. 2022) (Mitrano et al. 2021). Such machine learning algorithms require few computations and can be valuable tools if trained exhaustively, which is challenging for an in-space outfitting scenario. Conversely, finite element modeling can be leveraged with a polynomial approximation method such as B-splines to provide high fidelity models for a high computational cost (Lan and Shabana 2009) (Koessler et al. 2021).

PROBLEM DEFINITION

This section outlines the mathematical formulations for both the multibody and Cosserat rod representations of a single, uniform mass cable with constant diameter. The multibody and Cosserat-based model are both compared to a physical cable in a 2D plane.

The vector $\mathbf{p}^i_j$ is used to represent the translation to go from frame i to frame j. The special orthogonal group, $SO(3) \in \mathbb{R}^{3x3}$, contains orthonormal columns and can be used to represent orientation. The rotation matrix $\mathbf{R}^i_j \in SO(3)$ contains the rotation between frames i and j. The special Euclidean group $SE(3) \in \mathbb{R}^{4x4}$ builds about the rotation matrix to provide location and orientation of a given frame. The transformation matrix $\mathbf{T}^i_j \in SE(3)$ represents frame j relative to frame i and is equivalent to Eq. 1.

$$\mathbf{T}^i_j = \begin{bmatrix} \mathbf{R}^i_j & \mathbf{p}^i_j \\ 0 & 1 \end{bmatrix} \tag{1}$$

One important property to note about rotation and transformation matrices is that inverting the matrix flips the frame relationship. For example, $(\mathbf{R}^i_j)^{-1} = (\mathbf{R}^i_j)^T = \mathbf{R}^j_i$. This property is used heavily in both the multibody and Cosserat rod formulations, to relate cable segment frames relative to each other as well as to the global frame. For both models, the superscript frame i is often the spatial (global) frame, referred to as frame s.

Multibody formulation

The multibody formulation splits up the cable with mass m into n segments, where each segment has uniform mass $m_{link} = \frac{m}{n}$. Each link segment consists of two nodes, a base and forward node, as shown as dots in Figure 2. The forward node of the i^{th} segment connects to the base node of the $(i+1)^{th}$ segment via a multibody joint with the relative position and orientation dictated by rotational and linear springs. At the end of the cable, there is a $(n+1)$ spring set that connects the final link's forward node with the desired end position. The model is built parametrically to easily change the number of link segments for a given cable. By changing the number of links, there is

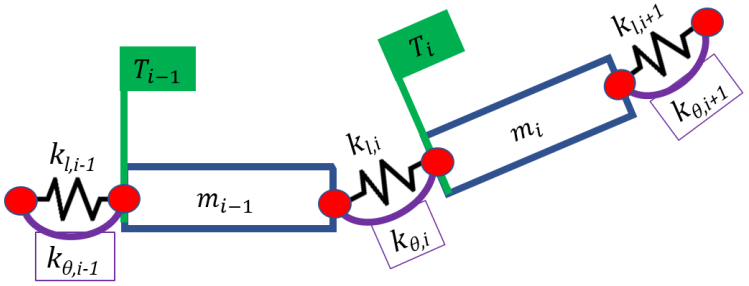

Fig. 2. Model definition with torsional and linear springs

direct control over the number of generalized coordinates required to generate a static solution via minimizing the potential energy in the cable as an optimization problem.

As the problem evaluated in this paper is 2D, each segment has one rotational spring evaluated along the central axis of the cable. The rotation matrix notation used throughout this model description is $\mathbf{R}(\theta_i)$ and indicates a rotation of θ_i in the 2D plane. The external force due to gravity, $m_{link}g$, acts in the $-y$ direction.

The spring deformation values can be combined into a single optimization variable vector $\mathbf{q}$, shown in Eq. 2, which represents the generalized coordinates of the multibody system. The spring deformation variables θ_i and δx_i represent the rotation and translation between the $(i-1)^{th}$ and i^{th} nodes, respectively, as in Figure 2.

$$\mathbf{q} = \begin{bmatrix} \mathbf{q}_1 & \dots & \mathbf{q}_{n+1} \end{bmatrix} \qquad \text{where } \mathbf{q}_i = \begin{bmatrix} \theta_i & \delta x_i \end{bmatrix} \text{ for } i = 1 \dots n+1 \tag{2}$$

The optimization problem is formulated using the cable potential energy as the cost function to be minimized, and includes potential energy terms for torsional springs, linear springs, and gravity acting at each link's center of mass (COM) as seen in Eq. 3.

$$U(\mathbf{q}) = \sum_{i=1}^{n} \frac{1}{2} k_r \theta_i^2 + \frac{1}{2} k_l \delta x_i^2 + m_{link} g y_i(\mathbf{q}) \tag{3}$$

Constants k_r and k_l represent the cable rotational and axial spring stiffness, respectively, and determined through system ID procedures for a specific cable. The global height of the link i COM, y_i, is a function of the optimization variables.

The location of the base node, $\mathbf{T}_i$, of a segment as shown in Figure 2 is given by Eq. 4.

$$\mathbf{T}_i^s = \mathbf{T}_{i-1}^s \mathbf{T}_{link} \mathbf{T}_{spr,i}^{link}(\theta_i, \delta x_i) \text{ for } i = 2 \dots n+1 \tag{4}$$

As the first link is connected to the origin and not a previous link, $\mathbf{T}_1^s = \mathbf{T}_{spr,1}^s(\theta_i, \delta x_i)$. $\mathbf{T}_{link}$ is the transformation that connects the two nodes of a link segment, from base node to forward node, creating a rigid body with mass m_{link} as indicated in Figure 2. $\mathbf{T}_{link}$ is a constant property of the cable and does not change between links. As such, the i subscript and the superscript term from the $\mathbf{T}$ notation is absent from these transformation matrices to emphasize that these frames are operators and are not to be treated as frames in the model by themselves.

The transformation matrix for a given spring relative to some frame a is as defined in Eq. 5.

$$\mathbf{T}_{spr,i}^a = \begin{bmatrix} \mathbf{R}(\theta_i) & \mathbf{p}_{spring,i} \\ \mathbf{0} & 1 \end{bmatrix} \qquad \mathbf{p}_{spring,i} = \mathbf{R}(\theta_i) \begin{bmatrix} \delta x_i \\ \mathbf{0} \end{bmatrix} \tag{5}$$

The position component $\mathbf{p}_{spring,i}$ is rotated internally because $\mathbf{T}^{a}_{spr,i}$ is *from* frame *a to* the spring frame - the linear deformation of the spring would not be applied axially without first applying the rotation of the spring. One end of the cable is fixed as a zero reference, and the desired end point is given by $\mathbf{p}_{des} = \begin{bmatrix} x_{des} & y_{des} & 0 \end{bmatrix}^T$. The propagated end of the cable is dependent on the generalized coordinate vector, and is the translational component of $\mathbf{T}_{n+1}$.

Utilizing the definitions above to describe the static goal configuration and contributions to potential energy, an optimization problem can be described as in Eq. 6. Sequential Quadratic Programming (SQP) via the Sequential Least SQuares Programming (SLSQP) solver in SciPy is used to solve this optimization problem (Virtanen et al. 2020).

$$\begin{aligned} \min_{\mathbf{q}} U(\mathbf{q}) &= \sum_{i=0}^{n} \frac{1}{2} k_r \theta_i^2 + \frac{1}{2} k_l \delta x_i^2 + m_{link} g y_i(\mathbf{q}) \\ \text{subject to } g(\mathbf{q}) &= |\mathbf{p}_n(\mathbf{q}) - \mathbf{p}_{des}| \leq \mathbf{0} \\ h(\mathbf{q}) &= \mathbf{p}_0 = \mathbf{0} \end{aligned} \tag{6}$$

The inequality constraint is the absolute value of the difference between the calculated and desired end positions, and is formatted in such a way as to assist the chosen solver, which has some hidden functionality due to using an external library. By formulating the static cable shape as an optimization problem, incorporating additional constraints for a feasible solution (collisions, additional goal points, etc.) is straightforward once defined.

Cosserat Elastic Rod Theory

The Cosserat rod approach takes advantage of known mechanical properties to generate force balance equations taking into account forces and torques due to *load-strain* and *torque-curvature* relations. For this formulation, the PyElastica open source library (Tekinalp et al. 2023) is used. The following section outlines the mathematical formulation for the continuous, shearable Cosserat rod, and the discretization process employed by PyElastica and detailed in Gazzola et al. (2018). PyElastica solves the static solution of the cable by applying the dynamic solver to the constraints and running it until the cable comes to rest.

The governing equations for the Cosserat rod of length l can be evaluated by considering the rod centerline, $s \in [0, l]$, at a given time, t, relative to a global frame. In the global frame, the cable position can be represented as $\mathbf{r}(s, t)$ and the orientation as rotation matrix $\mathbf{Q} = \mathbf{R_r}(s, t)$ (change in notation to align with Gazzola et al. (2018)).

The cable has known mechanical properties including cross-sectional area, density, Young's modulus, shear modulus, and second area moment of inertia. For this experiment some of the mechanical properties were approximated based on the physical cable composition. These mechanical properties can be combined to create the stiffness, $\mathbf{S} \in \mathbb{R}^{3x3}$, and bending, $\mathbf{B} \in \mathbb{R}^{3x3}$, matrices that compactly represent the internal *load-strain* and *torque-curvature* relationships as shown in Eq. 7.

$$\mathbf{n}(s) = \mathbf{S}\sigma(s) \quad \tau(s) = \mathbf{B}\kappa(s) \tag{7}$$

where $\mathbf{n}$ is the internal load relative to vector shear/stretch strain σ and τ is the internal torque due to curvature strain (bend and twist) κ, relative to the centerline. External loading can be split into force ($\mathbf{f}$) and torque ($\mathbf{c}$) components.

The scalar field $e(\hat{s}, \mathbf{t}) = \frac{ds}{d\hat{s}}$ represents the *local* dilation (stretch/compression) ratio relative to a reference configuration $\hat{s}$ and the tangent vector along the centerline $\mathbf{t}$. This dilation ratio, along

with the off axis rotation of the rod can be used to represent the local strain along the centerline via the relationship $\sigma = \mathbf{Q}(e\mathbf{t} - \mathbf{d}_3)$, where $\mathbf{d}_3$ is the column of $\mathbf{Q}$ that points perpendicular to the cross-section. The rod angular velocity ω and curvature κ at a local point are dependent on the rotation matrix $\mathbf{Q}$. Therefore, they are calculated as $[\omega] = (\frac{\partial}{\partial t}\mathbf{Q})^T\mathbf{Q}$ and $[\kappa] = (\frac{\partial}{\partial s}\mathbf{Q})^T\mathbf{Q}$, where $[\cdot]$ indicates a skew-symmetric operator on the contained vector.

The internal forces and torques of the Cosserat rod, with the external forcing from the vertical gravity vector, are applied to Newton's second law to calculate the translational and rotational accelerations for a given time step. The velocity relationships are easily obtained in the global frame. These equations combine to form the governing equations of the system, and are fully detailed in Gazzola et al. (2018).

Additional steps are implemented in the PyElastica library to discretize the continuous model to allow for timely computation. The spatial discretization evaluates internal and external forces over fixed sublengths of s, distributing forces between them. A time discretization allows the simulation to reach a stable orientation, PyElastica utilizes a second-order position Verlet time integrator. The constraints used to solve this problem involve fixing one end (constant position and orientation) and one pinned end (position only). The model would more accurately represent the cable with two fixed ends, but this additional constraint did not produce a valid solution in PyElastica.

RESULTS

In order to evaluate the performance of the different modeling methods, static configurations are found using the previously described formulations. The models are compared with each other to illustrate the changes in behavior for a changing number of states, and compared with a hardware experiment consisting of multiple static configurations.

For each link in the multibody system there are two variables in the 2 dimensional case, in addition to the variables necessary to track other constraints (such as end points); for the 3 dimensional case an additional 2 rotational springs are added. Conversely, the discrete Cosserat rod formulation requires 6 variables to track the full orientation and direction of each discretized segment. Model accuracy is evaluated using a physical cable in a static configuration. True cable shape is obtained using an Intel RealSense camera for RGB images. The test setup was erected using a uniform cable purchased off the shelf, utilizing a vertical test stand with evenly spaced markings and mounting fixtures. The vertical stand allowed gravity to be applied along a single axis to prescribe a single solution to the cable shape. The RGB image is processed using the OpenCV library (Bradski 2000), utilizing edge detection to isolate the cable as a contour in the image. Then, the Zhang-Suen thinning algorithm (Zhang and Suen 1984) is applied via the OpenCV *ximagproc* module to generate the cable centerline to compare against the simulated cables. Figure 3a illustrates the centerline resulting from the processing overlaid on the original hardware image.

To evaluate the accuracy of the multibody and Cosserat formulations to the hardware image, each point in the simulated model has an error associated with the *closest in magnitude* point on the cable. The differences between the hardware and simulated cables are fairly small, as indicated in Figure 3b. The multibody and Cosserat models deviate more from the hardware model than each other, however this may be due to challenges in constraining the orientation of the end position in the simulated models. The mean-square errors (MSE) to the hardware configuration shown in Figure 3 are summarized in Table 1, evaluating multiple discretization levels of the multibody model alongside the Cosserat formulation.

The data from this experiment points towards the Cosserat model providing a more accurate

Table 1. Comparison to hardware data

Simulation Model	Mean Square Error $[m^2]$
Cosserat Rod	6.531E-05
Multibody (n=5)	4.263E-03
Multibody (n=10)	2.010E-04
Multibody (n=20)	1.307E-04
Multibody (n=50)	2.292E-04

result. The multibody approach, while an order of magnitude higher in MSE still illustrates a fairly close tracking that could be well within the constraints of a robotic cable outfitting scenario. The $n = 20$ multibody case has a MSE of $5.134E-05\ [m^2]$ when compared to the Cosserat rod approximation for the case shown in Figure 3b, where there are 40 variables in the multibody solution compared to 240 variables in the Cosserat solution (discretization of 40 links in PyElastica).

The process used to identify the constant parameters for both the multibody and Cosserat models is not exhaustive, and it is evident when moving the cable in a quasi-static manner that the current values could be tweaked to better inform a dynamic model. Figure 4 shows the hardware and model approximations for various fixed locations. Ongoing work is being done to incorporate a classifier into the simulation to optimize the stiffness values based on errors with hardware data for both models. Part of the errors in this positioning is due to test setup and measurement of the cable, real-world approximation problems that are sure to arise in an in-space cable routing scenario.

CONCLUSION

This paper presents background into different state-of-the-art modeling methods for DLOs, and performs a simulated comparison of the two most prominent model-based methods: multibody and Cosserat rod formulations. The results of the simulations are compared to RGB images of a

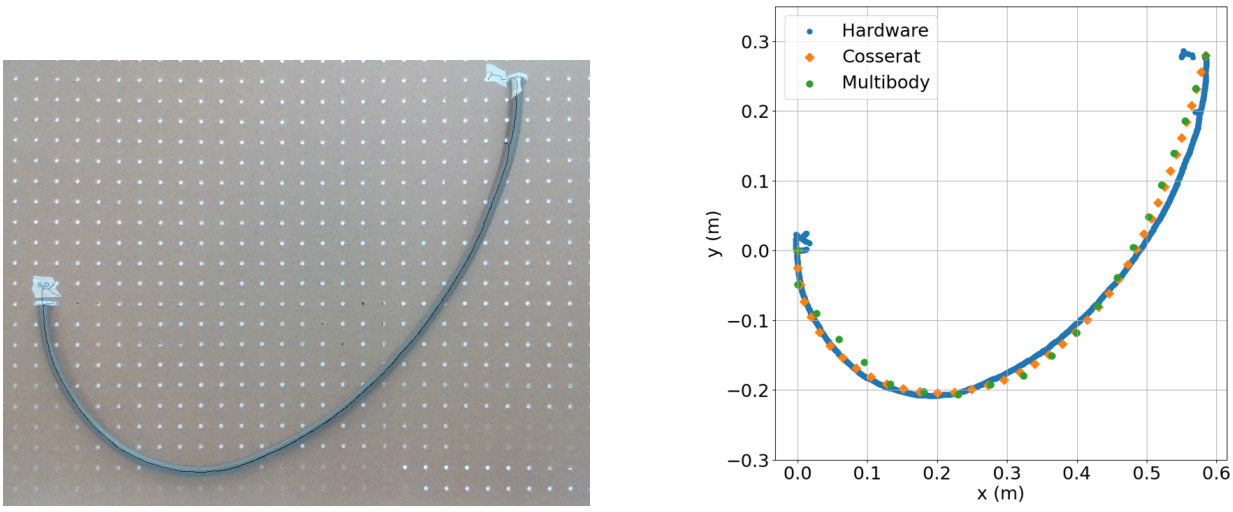

(a) **(b)**

Fig. 3. (a) Hardware setup with skeleton overlay, (b) Multibody and Cosserat modeling methods compared with cable RGB image.

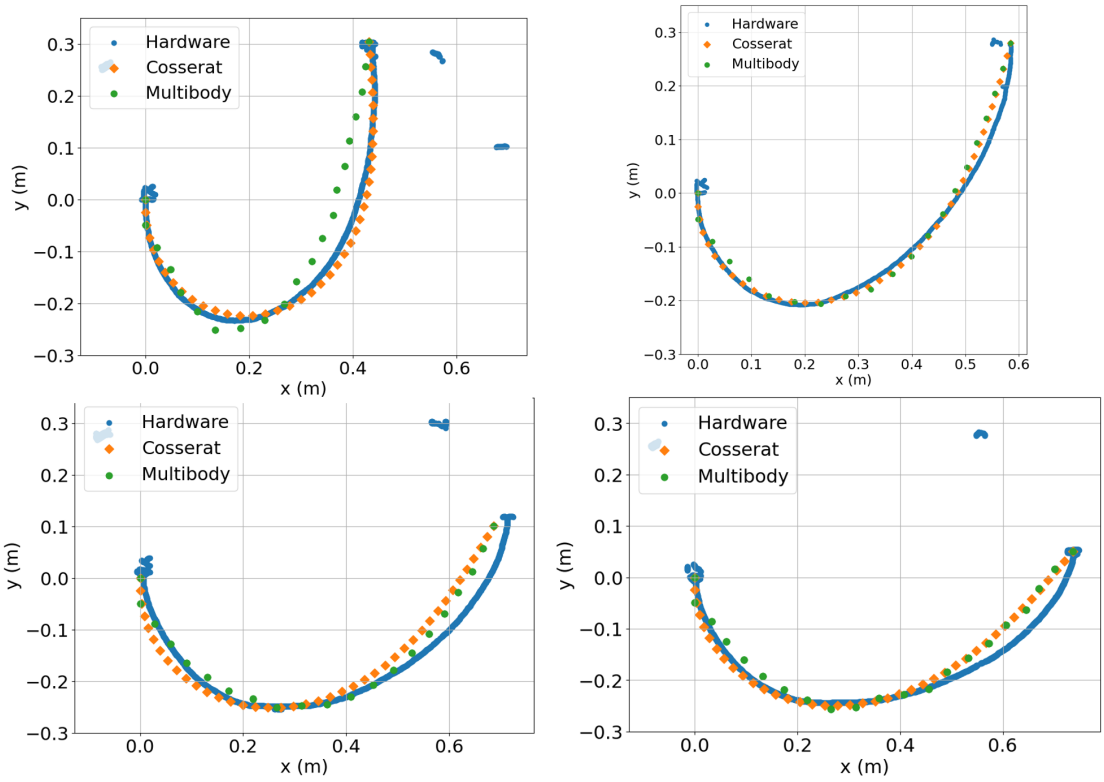

Fig. 4. Performance of multibody and Cosserat cable models for various cable positions.

cable. Both the low-state multibody approach and the high-state Cosserat rod approach are able to approximate the static cable shape, which indicates that the lower fidelity multibody approach is a valid modeling method for when medium accuracy is required for a cable routing scenario.

A fundamental evaluation such as this, evaluating different DLO modeling methods with an eye towards computational complexity, is necessary to advancing in-space outfitting and maintenance operations. Real-time control benefits from a minimum length state vector, allowing the autonomous system to react faster to deviations in the environment. A real-world outfitting scenario is likely to have many waypoints along the cable, in addition to bend constraints and collision volumes of a dense structural environment. The DLO itself must not bottleneck the control-loop; a slower control loop may not be responsive enough to avoid constraint violations of what could be a critical electrical component.

Ongoing work is focused on optimizing the parameters in the multibody model and comparing the 3D dynamics of the multibody model with the Cosserat model. Future work involves incorporating knowledge of a given scenario's constraints, and finding the minimum discretization necessary to reliably satisfy constraints. The resulting model can then be incorporated into a robotic system, aiding in the planning and real-time control of a DLO in a cluttered environment and enabling autonomous robotic cable routing of in-space facilities.

A viable control scheme is necessary to fully leverage robotic capabilities and establish a persistent presence on the lunar surface. Outfitting and maintenance are historically tasks that have not seen much automation. This approach which must change in order for a lunar facility that is not continuously crewed to operate effectively.

NOTATION

The following symbols are used in this paper:

e = cable dilation ratio
$\mathbf{f}, \mathbf{c}$ = force and torque vectors $\in \mathbb{R}^3$
g = gravity constant $\left[\frac{m}{s^2}\right]$
k_θ = rotational (torsional) spring constant $\left[\frac{N}{rad}\right]$
k_l = linear spring constant $\left[\frac{N}{m}\right]$
l = total length of cable $[m]$
m = total mass of cable $[kg]$
m_{link} = mass of single link $[kg]$
n = number of link segments per cable
$\mathbf{p}_i, \mathbf{r}$ = position vectors $\in \mathbb{R}^3$
q = optimization variables
$\mathbf{R}^i_j$ = $SO(3)$ rotation matrix $\in \mathbb{R}^{3x3}$
s = point on parametric line
$\hat{s}$ = point on rest reference line $\in [0, l]$
$\mathbf{T}^i_j$ = $SE(3)$ transformation matrix $\in \mathbb{R}^{4x4}$
U = potential energy $[J]$
θ = relative rotation $[rad]$
δx = deformation of linear spring $[m]$
σ = linear strain $\in \mathbb{R}^3$
κ = curvature strain $\in \mathbb{R}^3$
ω = angular velocity $\in \mathbb{R}^3$

ACKNOWLEDGMENTS

This work was supported by a NASA Space Technology Graduate Research Opportunity (80NSSC21K1286).

REFERENCES

Belvin, W. K., Doggett, W. R., Watson, J. J., Dorsey, J. T., Warren, J. E., Jones, T. C., Komendera, E. E., Mann, T., and Bowman, L. M. (2016). "In-Space Structural Assembly: Applications and Technology." *3rd AIAA Spacecraft Structures Conference*, San Diego, California, USA, American Institute of Aeronautics and Astronautics, <http://arc.aiaa.org/doi/10.2514/6.2016-2163> (January).

Bradski, G. (2000). "The OpenCV Library." *Dr. Dobb's Journal of Software Tools*.

Everson, H., Moser, J., Quartaro, A., Glassner, S., and Komendera, E. (2020). "Autonomous Multi-Robot Assembly of Solar Array Modules: Experimental Analysis and Insights." *2020 IEEE/RSJ International Conference on Intelligent Robots and Systems (IROS)*, IEEE (October).

Gazzola, M., Dudte, L. H., McCormick, A. G., and Mahadevan, L. (2018). "Forward And Inverse Problems In The Mechanics Of Soft Filaments." *Royal Society Open Science*, 5(6), 171628.

Govindaraj, S., Gancet, J., Urbina, D., Brinkmann, W., Aouf, N., Lacroix, S., Wolski, M., Colmenero, F., Walshe, M., Ortega, C., and Bodo, B. (2019). "PRO-ACT: Planetary Robots Deployed For Assembly And Construction Of Future Lunar ISRU And Supporting Infrastructures." *Advanced Space Technologies in Robotics and Automation (ASTRA) 2019* (May).

Hermansson, T., Bohlin, R., Carlson, J. S., and Söderberg, R. (2013). "Automatic Assembly Path Planning for Wiring Harness Installations." *Journal of Manufacturing Systems*, 32(3), 417–422.

ICON Technology (2022). "ICON To Develop Lunar Surface Construction System With $57.2 Million NASA Award." Accessed 9/8/2023, <www.iconbuild.com/newsroom/icon-to-develop-lunar-surface-construction-system-with-57-2-million-nasa-award> (November).

Iwamura, S., Mizukami, Y., Endo, T., and Matsuno, F. (2022). "Cable-path Optimization Method for Industrial Robot Arms." *Robotics and Computer-Integrated Manufacturing*, 73, 102245.

Jin, S., Lian, W., Wang, C., Tomizuka, M., and Schaal, S. (2022). "Robotic Cable Routing with Spatial Representation." *IEEE Robotics and Automation Letters*, 7(2), 5687–5694.

Karumanchi, S., Edelberg, K., Nash, J., Bergh, C., Smith, R., Emanuel, B., Carlton, J., Koehler, J., Kim, J., Mukherjee, R., Kennedy, B., and Backes, P. (2018). "Payload-Centric Autonomy for In-Space Robotic Assembly of Modular Space Structures." *Journal of Field Robotics*, 35(6), 1005–1021 _eprint: https://onlinelibrary.wiley.com/doi/pdf/10.1002/rob.21792.

Koessler, A., Filella, N. R., Bouzgarrou, B., Lequievre, L., and Ramon, J.-A. C. (2021). "An Efficient Approach To Closed-Loop Shape Control of Deformable Objects Using Finite Element Models." *2021 IEEE International Conference on Robotics and Automation (ICRA)*, IEEE (May).

Kugelstadt, T. and Schömer, E. (2016). "Position and Orientation Based Cosserat Rods." *Eurographics/ ACM SIGGRAPH Symposium on Computer Animation*.

Lan, P. and Shabana, A. A. (2009). "Integration of B-Spline Seometry and ANCF Finite Element Analysis." *Nonlinear Dynamics*, 61(1-2), 193–206.

Liu, F., Su, E., Lu, J., Li, M., and Yip, M. C. (2023). "Robotic Manipulation of Deformable Rope-Like Objects Using Differentiable Compliant Position-Based Dynamics." *IEEE Robotics and Automation Letters*, 8(7), 3964–3971.

Lv, N., Liu, J., and Jia, Y. (2022). "Dynamic Modeling and Control of Deformable Linear Objects for Single-Arm and Dual-Arm Robot Manipulations." *IEEE Transactions on Robotics*, 38(4), 2341–2353.

Lv, N., Liu, J., Xia, H., Ma, J., and Yang, X. (2020). "A Review of Techniques for Modeling Flexible Cables." *Computer-Aided Design*, 122, 102826.

Mitrano, P., MConachie, D., and Berenson, D. (2021). "Learning Where To Trust Unreliable Models In An Unstructured World for Deformable Object Manipulation." *Science Robotics*, 6(54).

Moll, M. and Kavraki, L. (2006). "Path Planning for Deformable Linear Objects." *IEEE Transactions on Robotics*, 22(4), 625–636.

Moses, R. W. and Mueller, R. P. (2021). "Requirements Development Framework for Lunar In Situ Surface Construction of Infrastructure." *Earth and Space 2021*, 1141–1155, <https://ascelibrary.org/doi/abs/10.1061/9780784483374.106>.

NASA (2020). "Automated Reconfigurable Mission Adaptive Digital Assembly Systems (ARMADAS)." Accessed 10/4/2023, <https://www.nasa.gov/centers-and-facilities/langley/automated-reconfigurable-mission-adaptive-digital-assembly-systems-armadas/> (April).

NASA (2022a). "MOON TO MARS OBJECTIVES." Accessed 8/3/2023, <https://www.nasa.gov/sites/default/files/atoms/files/m2m-objectives-exec-summary.pdf> (September).

NASA (2022b). "OSAM-1 Mission On-orbit Servicing, Assembly, and Manufacturing 1." Accessed 9/26/2023, <https://nexis.gsfc.nasa.gov/osam-1.html>.

Saha, M. and Isto, P. (2007). "Manipulation Planning for Deformable Linear Objects." *IEEE*

Transactions on Robotics, 23(6), 1141–1150.

Sanchez, J., Corrales, J.-A., Bouzgarrou, B.-C., and Mezouar, Y. (2018). "Robotic Manipulation and Sensing of Deformable Objects in Domestic and Industrial Applications: A Survey." *The International Journal of Robotics Research*, 37(7), 688–716.

Shah, A., Blumberg, L., and Shah, J. (2018). "Planning for Manipulation of Interlinked Deformable Linear Objects With Applications to Aircraft Assembly." *IEEE Transactions on Automation Science and Engineering*, 15(4), 1823–1838.

Song, K., Mikulas, M., Mahlin, M. K., and Cassady, J. T. (2023). "Sizing and Design Tool for Tall Lunar Tower." *AIAA SCITECH 2023 Forum*, American Institute of Aeronautics and Astronautics (January).

Suzuki, R., Okada, Y., Yokota, Y., Saijo, T., Eto, H., Sakai, Y., Murano, K., Ohno, K., Tadakuma, K., and Tadokoro, S. (2022). "Cooperative Towing by Multi-Robot System That Maintains Welding Cable in Optimized Shape." *IEEE Robotics and Automation Letters*, 7(4), 11783–11790.

Tekinalp, A., Kim, S. H., Bhosale, Y., Parthasarathy, T., Naughton, N., Nasiriziba, I., Cui, S., Stölzle, M., Shih, C.-H. C., and Gazzola, M. (2023). "GazzolaLab/PyElastica: v0.3.1 (May).

Tummers, M., Lebastard, V., Boyer, F., Troccaz, J., Rosa, B., and Chikhaoui, M. T. (2023). "Cosserat Rod Modeling of Continuum Robots from Newtonian and Lagrangian Perspectives." *IEEE Transactions on Robotics*, 39(3), 2360–2378.

Virtanen, P., Gommers, R., Oliphant, T. E., Haberland, M., Reddy, T., Cournapeau, D., Burovski, E., Peterson, P., Weckesser, W., Bright, J., van der Walt, S. J., Brett, M., Wilson, J., Millman, K. J., Mayorov, N., Nelson, A. R. J., Jones, E., Kern, R., Larson, E., Carey, C. J., Polat, İ., Feng, Y., Moore, E. W., VanderPlas, J., Laxalde, D., Perktold, J., Cimrman, R., Henriksen, I., Quintero, E. A., Harris, C. R., Archibald, A. M., Ribeiro, A. H., Pedregosa, F., van Mulbregt, P., and SciPy 1.0 Contributors (2020). "SciPy 1.0: Fundamental Algorithms for Scientific Computing in Python." *Nature Methods*, 17, 261–272.

Waltz, W. J., Grande, M. L., and Moses, R. W. (2022). "Autonomous System Operations for Lunar Safe Haven Establishment and Sustainment." *AIAA SCITECH 2022 Forum*, American Institute of Aeronautics and Astronautics (January).

Yu, M., Lv, K., Wang, C., Tomizuka, M., and Li, X. (2023). "A Coarse-to-Fine Framework for Dual-Arm Manipulation of Deformable Linear Objects with Whole-Body Obstacle Avoidance." *2023 IEEE International Conference on Robotics and Automation (ICRA)*, IEEE (May).

Zhang, T. Y. and Suen, C. Y. (1984). "A Fast Parallel Algorithm for Thinning Digital Patterns." *Communications of the ACM*, 27(3), 236–239.